

pubs.acs.org/bc Article

# Combining Doxorubicin-Conjugated Polymeric Nanoparticles and 5-Aminolevulinic Acid for Enhancing Radiotherapy against Lung Cancer

Jinghua Han, Wei Yang, Yuanke Li, Jianwen Li, Fangchao Jiang, Jin Xie,\* and Xinglu Huang\*



Cite This: Bioconjugate Chem. 2022, 33, 654-665



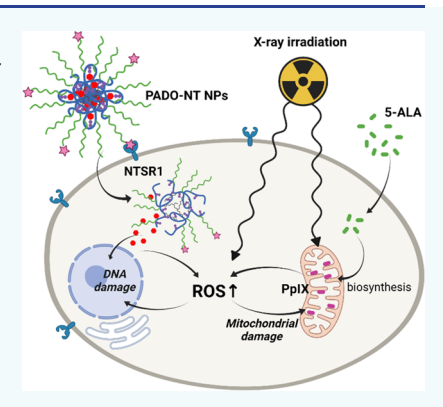
ACCESS I

Metrics & More

Article Recommendations

Supporting Information

**ABSTRACT:** Radiation therapy (RT) concurrent with chemotherapy improves local lung cancer control but may cause systemic toxicity. There is an unmet clinical need of treatments that can selectively sensitize cancer cells to RT. Herein, we explored a radiosensitizing strategy that combines doxorubicin (DOX)-encapsulated polyaspartamide nanoparticles and 5-aminolevulinic acid (5-ALA). The DOX-polyaspartamide nanoparticles were coupled with NTS<sub>mut</sub>, a ligand specific to neurotensin receptor type 1 (NTSR1), for lung cancer targeting. DOX was coupled to the polymer backbone through a pH-sensitive hydrazone linker, which allows for controlled release of the drug in an acidic tumor micromovement. Meanwhile, 5-ALA accumulates in the cancer cell's mitochondria, forming protoporphyrin (PpIX) that amplifies RT-induced oxidative stress. When tested in vitro in H1299 cells, DOX-encapsulated nanoparticles in conjugation with 5-ALA enhanced cancer cell killing owing to the complementary radiosensitizing effects of DOX and 5-ALA. In vivo studies confirmed that the combination improved tumor suppression relative to RT alone without causing toxicity to normal tissues. Overall, our study suggests an effective and selective radiosensitizing approach.



ung cancer is the leading cause of cancer-related death. ✓ Every year, lung cancer claims the lives of approximately 1.8 million people, which account for 18.0% of the total cancer deaths. It is also the second most commonly diagnosed cancer type, with an estimated 2.2 million new cases (11.4% of total cases) diagnosed in the year 2020 alone. About 85% of lung cancer cases belong to the non-small cell lung cancer (NSCLC) subtype.<sup>2</sup> Surgical resection is the recommended treatment for early-stage NSCLC.3 However, the majority of the patients (75%) are diagnosed at an advanced stage (stage III/IV). Radiation therapy (RT) is a standard treatment when cancer is localized. RT utilizes high-energy photon beams, which induce reactive oxygen species (ROS) and oxidative damages to biomolecules including DNA, causing cancer cell death. 5-7 The maximum cumulative radiation dose is 60-70 Gy for NSCLC,8 restricted by normal tissue toxicity. RT with concurrent chemotherapy may improve local control and patient survival.9 However, efficacy and patient eligibility are limited by systemic toxicity caused by chemotherapy. There is an unmet clinical need of new treatments that can effectively and selectively sensitize tumors to RT.

Herein, we explored a novel radiosensitizing strategy that combines doxorubicin (DOX)-loaded nanoparticles and 5aminolevulinic acid (5-ALA) (Scheme 1). Specifically, we polymerized L-aspartic acid into polysuccinimide (PSI) and then grafted onto the polymer backbone octadecylamine, MPEG5000-NH2, and DOX, producing an amphiphilic polymer, PADO-MPEG, which self-assembles into nanoparticles (PADO NPs). For tumor targeting, we conjugated NTS<sub>mut</sub>, a tumor targeting ligand, onto the nanoparticles. We hypothesize that the resulting nanoparticles, designated as PADO-NT NPs, can accumulate in tumors after systemic administration and release DOX therein. Concurrent with PADO-NT NPs, we also administer 5-ALA, an amino acid precursor of protoporphyrin IX (PpIX). 5-ALA was traditionally employed as a photosensitizer but has shown benefits in enhancing RT in recent studies. 11,12 DOX is a commonly used chemotherapeutic agent and has shown to be able to enhance radiotherapy. 13-17 DOX damages DNA by intercalation and complexation with topoisomerase II, 18,19 whereas 5-ALA targets mitochondria, disrupting its functions and promoting production of secondary radicals.<sup>20</sup> We reason that the two modalities can synergize to boost RT-induced tumor suppression.

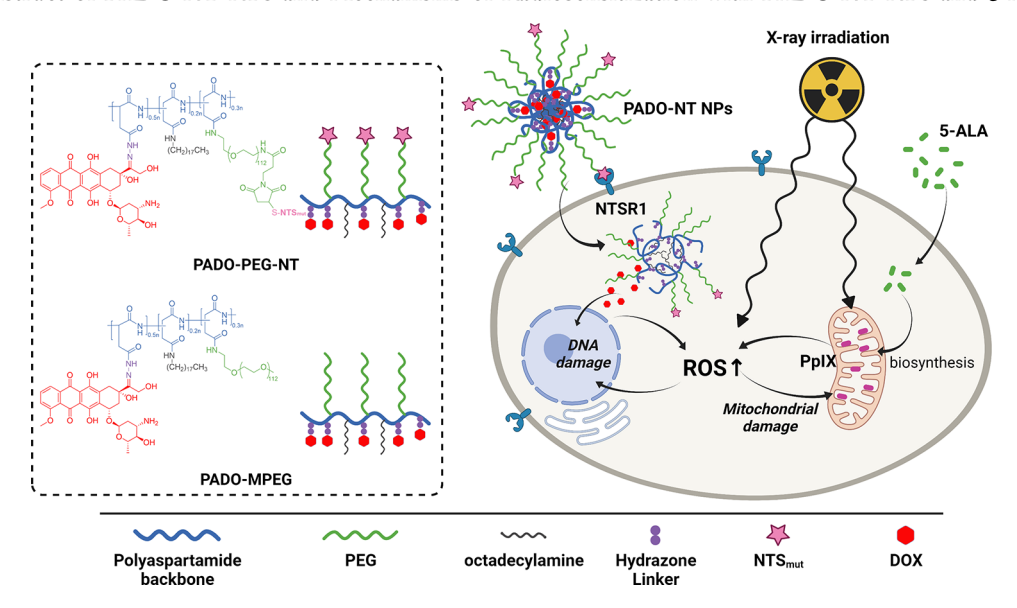
We anticipate high tumor selectivity of the approach. This is attributed to (i) NTS<sub>mut</sub> as a tumor targeting ligand. NTS<sub>mut</sub> binds to neurotensin receptor type 1 (NTSR1). Recent studies

Received: February 6, 2022 March 22, 2022 Revised: Published: April 6, 2022





Scheme 1. Construct of PADO-NT NPs and Mechanisms of Radiosensitization with PADO-NT NPs and 5-ALA<sup>a</sup>



"PADO-MPEG and PADO-PEG-NT were mixed at a 2:1 ratio, forming PADO-NT NPs that target NTSR1 overexpressed on cancer cells. Under an acidic tumor microenvironment, the hydrazone bond is cleaved, releasing DOX that causes DNA damage. Meanwhile, PpIX forms and accumulates in cancer cells' mitochondria, which under radiation promote ROS production. The two components synergize to enhance radiation-induced cell death.

show that NTSR1 is positive in 59.7% of lung cancer patients. NTSR1 expression is strongly associated with a worse 5 year overall survival and relapse-free survival. Meanwhile, NTSR1 is expressed at low or undetectable levels in healthy lung tissues, making it an appealing target for targeted therapies. Note that neurotensin, the wildtype NTSR1 ligand, has a short half-life *in vivo* due to its high susceptibility to peptidase degradation. NTS<sub>mut</sub> solves the problem by replacing the L-isoleucine with an unnatural amino acid (L-tert-leucine). Compared to wildtype neurotensin, NTS<sub>mut</sub> showed comparable NTSR1 affinity but significantly improved stability. 22

(ii) Hydrazone as a pH-sensitive linker. DOX is covalently coupled to the PSI backbone using hydrazone as a linker. While hydrazone is stable at physiological pH, the bond is cleaved when the pH is below 6.0. This property is exploited to enable selective release of DOX in the acidic tumor microenvironment. (iii) Intrinsic tumor targeting ability of 5-ALA. 5-ALA is the sole biosynthetic precursor of PpIX. Lacking ferrochelatase, cancer cells are slow in converting PpIX to heme, causing PpIX to accumulate in the mitochondria. Recent studies suggest that PpIX can amplify RT-induced radical production in the mitochondria and exacerbate oxidative stress of cells, thereby enhancing the efficacy of RT. (20,28–30)

We investigated the synthesis of PADO-NT NPs and tested their stability and drug release in solutions. We then evaluated the efficacy of the PADO-NT NPs and-5-ALA combination *in vitro* with H1299 cells. Last, we evaluated the efficacy and the safety of the combinational approach *in vivo* in an H1299 xenograft model.

#### RESULTS AND DISCUSSION

**Synthesis and Characterizations of PADO-MPEG and PADO-PEG-NT.** The synthesis steps of PADO-MPEG and PADO-PEG-NT are illustrated in Figure 1. The structure of the PSI polymer and the conjugates were characterized by <sup>1</sup>H

NMR spectroscopy. PSI was synthesized by acid-catalyzed polycondensation according to a published protocol.<sup>31</sup> The <sup>1</sup>H NMR spectra in Figure S1 confirm the successful synthesis of PSI, finding peaks at  $\delta$  5.26, 3.18, and 2.71 ppm, which correspond to hydrogen atoms on the succinimidyl rings. The molecular weight of PSI was determined by gel permeation chromatography (GPC) in DMF (Mn = 19,638 Da, Mw = 36,721 Da, PDI = 1.87).

NT-PEG-NH<sub>2</sub> was synthesized by Michael addition linking the cysteine group of Cys-NTS<sub>mut</sub> to MAL-PEG-NH<sub>2</sub>.  $^1\mathrm{H}$  NMR found peaks at  $\delta$  7.20–6.60, 3.30–2.50, and 0.90–0.75 ppm, which are attributable to tyrosine, lysine, tert-leucine, and leucine of NTS<sub>mut</sub> (Figure S2). The maleimide peaks disappeared after the coupling, supporting the successful conjugation. By analyzing free Cys-NTS<sub>mut</sub> before and after conjugation by high-performance liquid chromatography (HPLC) (Figure S3), it was determined that the conjugation yield was 68%.

Next, octadecylamine, MPEG-NH<sub>2</sub> or NT-PEG-NH<sub>2</sub>, and an excess amount of hydrazine monohydrate were mixed and conjugated to the polymer through a ring-opening reaction, producing PAO-MPEG or PAO-PEG-NT. Characteristic peaks belonging to octadecylamine, PEG, hydrazide, amino acid residuals, and amide were identified in the conjugates (Figures S4 and S5). Meanwhile, peaks corresponding to the PSI ring vanished (Figures S4 and S5). Last, DOX was conjugated to the copolymer through a hydrazone linker, evidenced by peaks at  $\delta$  7.99–7.44 and 5.51–4.16 ppm on the <sup>1</sup>H NMR spectrum (Figures S6 and S7).

The optimal ratio between DOX and MPEG was investigated. Briefly, we varied the ratio between MPEG and DOX (MPEG10%-DOX70%, MPEG20%-DOX60%, and MPEG30%-DOX50%) while keeping the percentage of octadecylamine consistent at 20%. Size change for the resulting nanoparticles was monitored by DLS (Figure S9). While nanoparticles formed with MPEG10%-DOX70% and MEPG20%-DOX60% showed a relatively wide size distribu-

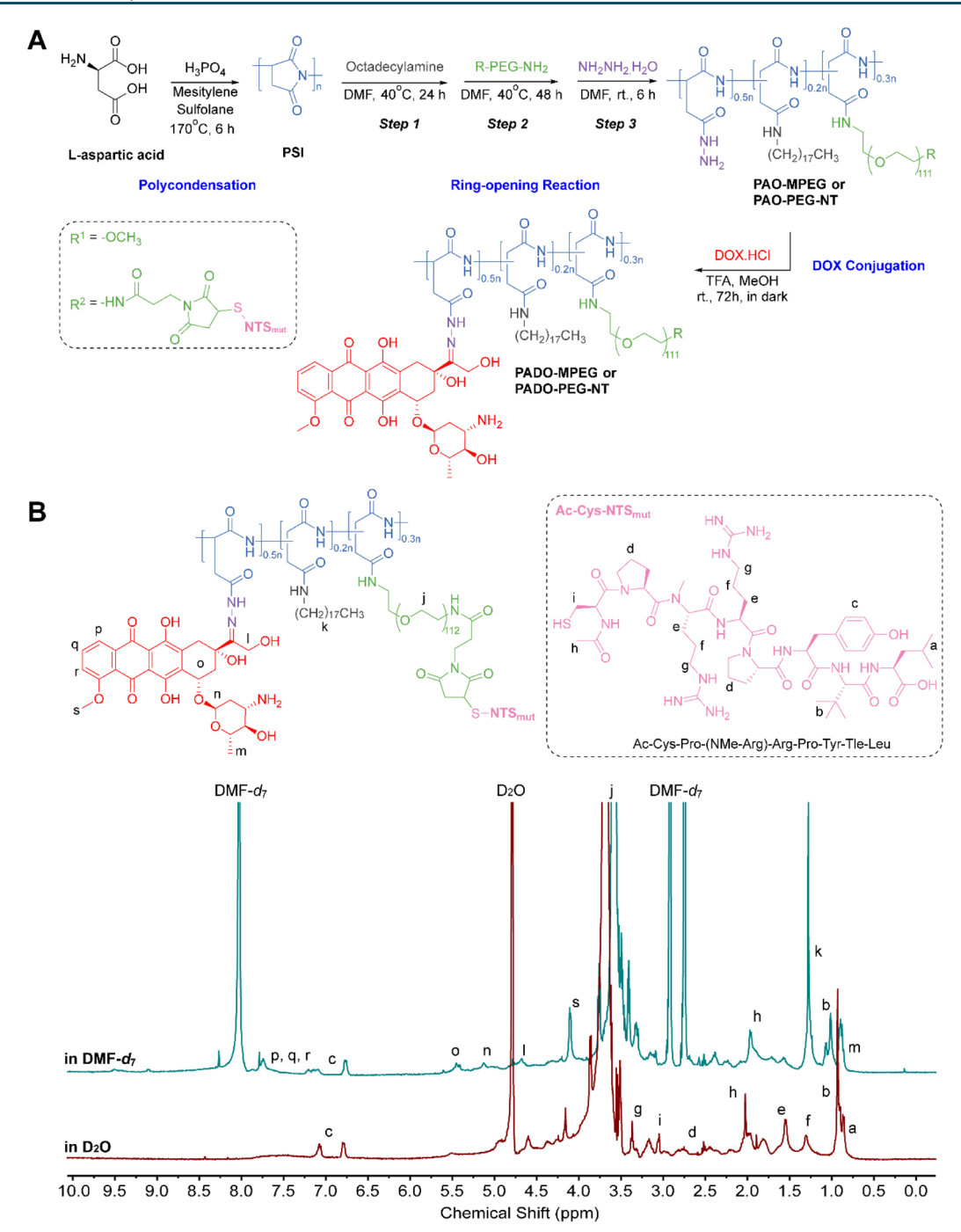


Figure 1. (A) Synthetic route for PADO-MEPG and PADO-PEG-NT. (B)  $^{1}$ H NMR spectra of PADO-PEG-NT in DMF- $d_{7}$  (green) and D<sub>2</sub>O (red).

tion, those formed with MEPG30%-DOX50% showed minimum size change over time, indicating good colloidal stability. Hence, MEPG30%-DOX50% was chosen for subsequent studies. We also measured the critical aggregation concentration (CAC) of PADO-MPEG and PADO-NT by dynamic light scattering (DLS) (count rates vs polymer concentrations). Both polymer conjugates displayed low CACs (16.82 and 15.57  $\mu$ g/mL, respectively), confirming their ability to form nanoparticles (Figure S10).

Preparation of PADO NPs and PADO-NT NPs. PADO-MPEG readily disperses in PBS, forming nanoparticles (PADO NPs). Their hydrodynamic size was 110.6 nm (Figure 2A). Mixing PADO-MPEG and PADO-PEG-NT forms nano-

particles with slightly larger sizes of 127.6 nm (PADO-NT NPs, Figure 2B,C; only nanoparticles made of PADO-MPEG and PADO-PEG-NT at a 2:1 molar ratio were shown). The size increase was due to NTS<sub>mut</sub> on the particle surface. Formation of nanoparticles was also supported by <sup>1</sup>H NMR of PADO-PEG-NT (Figure 1B) and PADO-MPEG (Figure S8) in D<sub>2</sub>O. Compared to <sup>1</sup>H NMR spectra taken in DMF-d<sub>7</sub>, characteristic peaks belonging to the hydrophobic components (DOX and octadecylamine) were almost undetectable, while peaks from NTS<sub>mut</sub> were elevated. This was because the NTS<sub>mut</sub> presets on the surface, whereas DOX and octadecylamine are encapsulated into the core of the nanoparticles. Transmission electron microscopy (TEM) and scanning

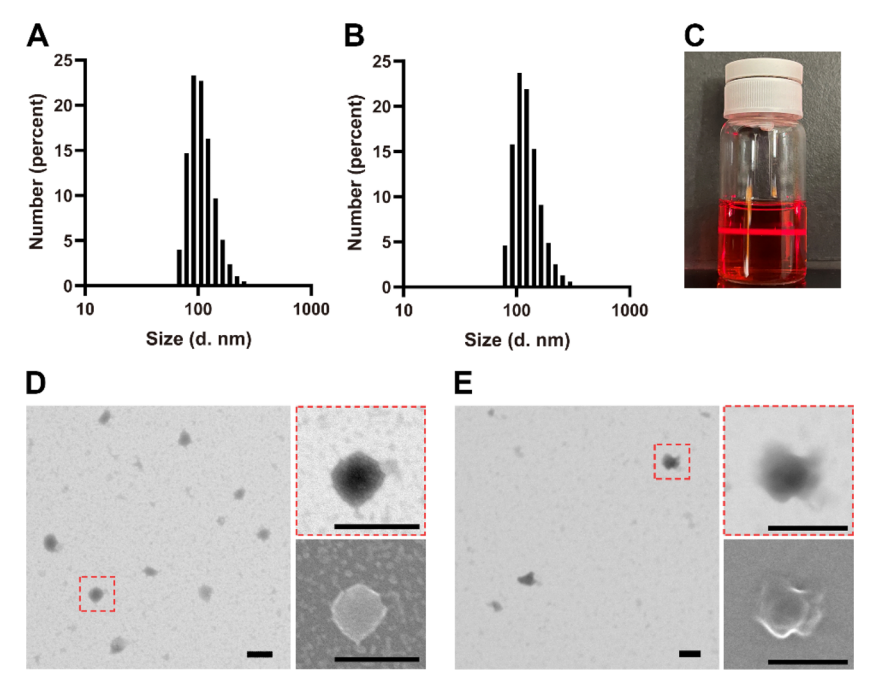


Figure 2. Hydrodynamic sizes of (A) PADO NPs and (B) PADO-NT NPs, measured in PBS (pH = 7.4) by DLS. (C) Solution of PADO-NT NPs showing a Tyndall effect under light radiation. Representative TEM images of (D) PADO NPs and (E) PADO-NT NPs. Upper right: zoomed-in TEM images of a single PADO NP or PADO-NT NP; lower right: SEM images of the nanoparticles. Scale bars, 200 nm.

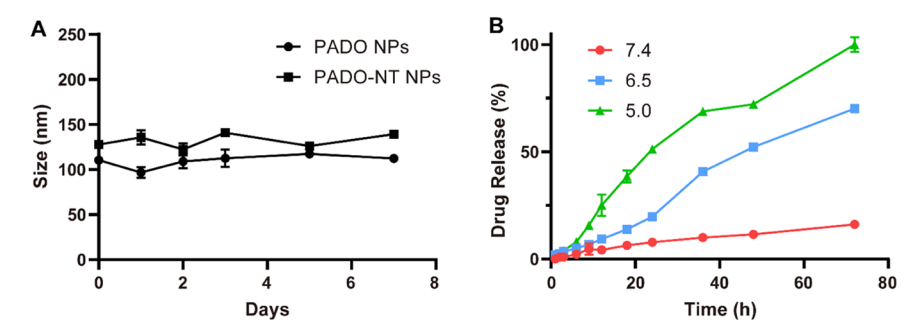


Figure 3. (A) Colloidal stability of PADO NPs and PADO-NT NPs, evaluated by monitoring nanoparticle size changes in PBS (pH = 7.4). (B) DOX release from PADO NPs, measured in PBS (pH = 7.4 or 6.5) and sodium acetate buffer (pH = 5.0) at 37 °C.

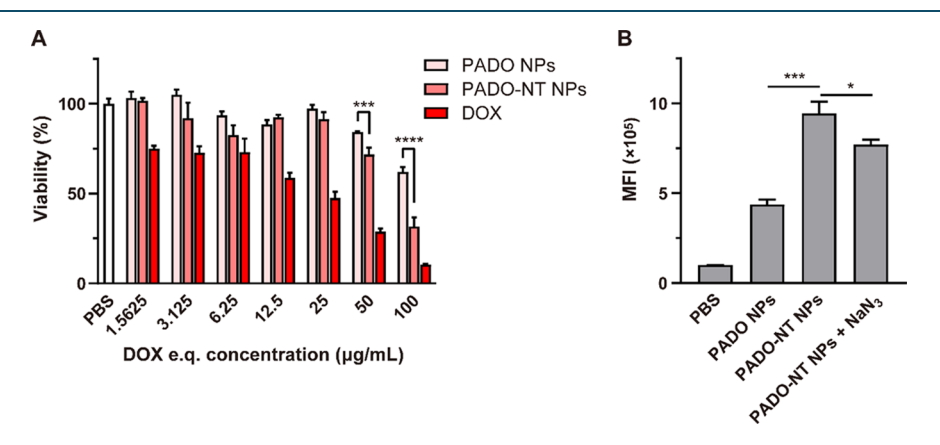


Figure 4. (A) In vitro cytotoxicity study, measured by the ATP bioluminescence assay. PADO NPs, PADO-NT NPs, or DOX at a DOX e.g. concentration of  $1.5625-100~\mu g/mL$  was incubated with H1299 cells in the absence of radiation. Viability was measured after 24 h. PBS was tested as a control. (B) Cell uptake. PADO NPs, PADO-NT NPs, or PADO-NT NPs + NaN<sub>3</sub> (e.q. DOX concentration of  $50~\mu g/mL$  for PADO NPs and PADO-NT NPs; the NaN<sub>3</sub> concentration was 50~mM) were incubated with H1299 cells. After 2 h, mean fluorescence intensity of DOX was measured by flow cytometry. Trypan blue was applied to quench DOX non-specifically associated to the plasma membrane. PBS-treated cells were measured as a control. \*p < 0.05; \*\*\*\*p < 0.001; \*\*\*\*\*p < 0.0001.

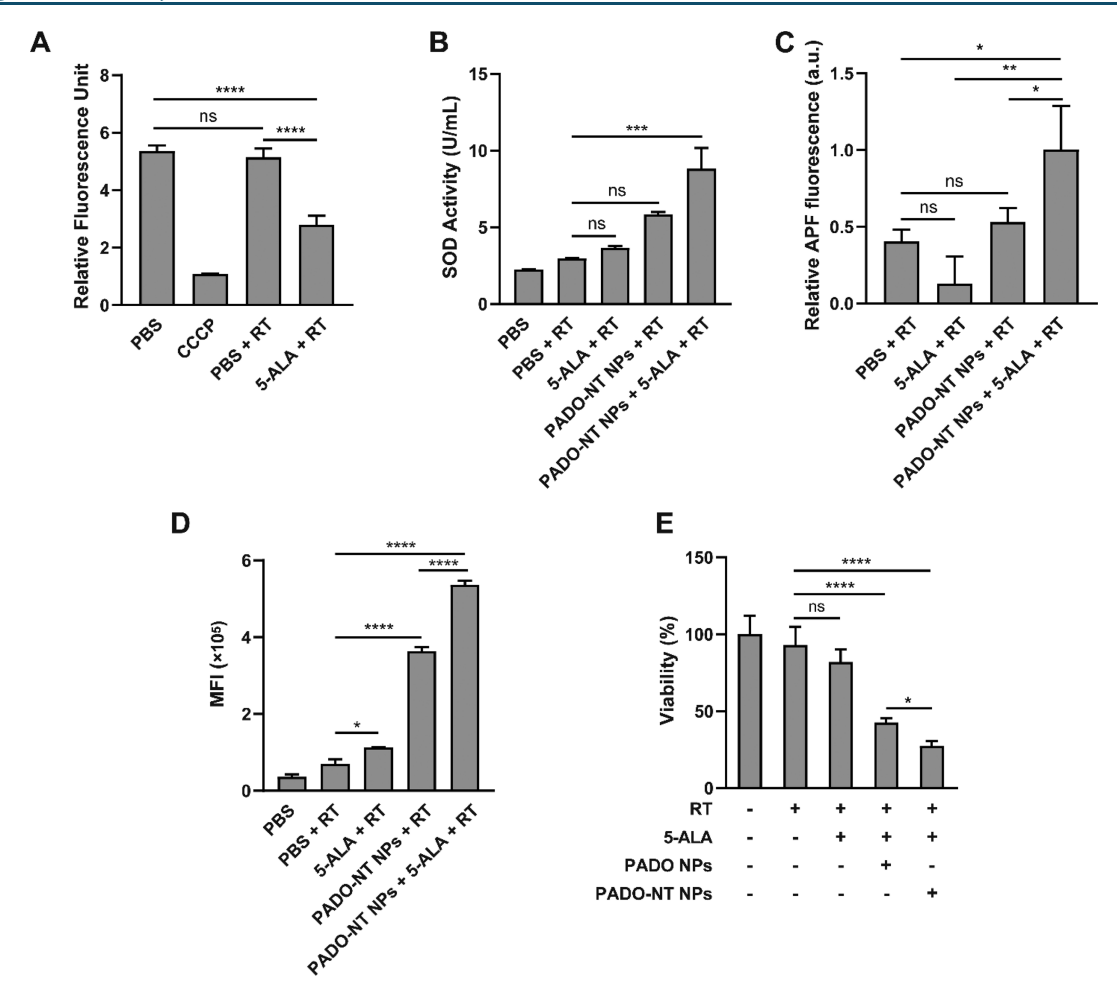


Figure 5. Evaluating radiation sensitizing effects *in vitro*. (A) Mitochondria membrane potential ( $\Delta \Psi_{\rm m}$ ), measured by the JC-1 assay. 5-ALA (1 mM) was incubated with H1299 cells. Radiation (5 Gy) was applied 3 h later. JC-1 staining was performed at 24 h. For comparison, carrier only (PBS) and carrier plus RT (PBS + RT) were examined. Carbonyl cyanide 3-chlorophenylhydrazone (CCCP) was tested as a positive control. (B–E) Radiosensitizing effects of 5-ALA and PADO-NT NPs. 5-ALA (1 mM) and PADO NPs or PADO-NT NPs (e.q. DOX concentration of 50 μg/mL) were incubated with H1299 cells. Radiation (5 Gy) was applied after 3 h. (B) SOD activity, measured by a superoxide dismutase activity colorimetric assay kit 1 h after radiation. (C) ROS level, assessed with APF. Fluorescence intensities of APF were measured and normalized to the unirradiated controls. (D) Double-strand breaks, measured by anti-γH2AX staining using flow cytometry 4 h after radiation. Mean fluorescence intensity (MFI) was recorded and compared. (E) Viability under radiation, measured by the ATP bioluminescence assay 24 h after radiation. \*p < 0.05; \*\*p < 0.01; \*\*\*p < 0.001; \*\*\*\*p < 0.0001; ns, no significant difference.

electron microscopy (SEM) found nanoparticles of similar sizes (Figure 2D,E). Zeta potentials of PADO NPs and PADO-NT NPs were  $1.25 \pm 0.05$  and  $0.78 \pm 0.07$  mV, respectively; the difference was again attributed to NTS<sub>mut</sub> present on particles in the latter formulation. Drug loading capacities (LCs %) were 12.6 and 9.7%, for PADO NPs and PADO-NT NPs, respectively. These values are close to the theoretical maximum, which is calculated to be 14%.

Colloidal Stability and Drug Release. The colloidal stability was evaluated by monitoring nanoparticle size change in PBS (pH 7.4) using DLS. Both PADO NPs and PADO-NT NPs showed minimal size change over a week (Figure 3A). Drug release was investigated in buffer solutions with pH 7.4, 6.5, and 5.0 at 37 °C (Figure 3B). At pH 7.4, less than 17% of the DOX was released from PADO NPs after 72 h. By contrast, more than 70% of the DOX was released at pH 6.5 and all of the payload was liberated at 5.0 by 72 h. The drug release is caused by the cleavage of the hydrazone bond, which is pH-sensitive. This observation supports the notion that nanoparticles can remain intact in the blood circulation and

selectively release DOX in the acidic tumor milieu or inside the late endosomes/lysosomes of cancer cells. Note that DOX release is also temperature-dependent as minimal drug leakage was found when PADO NPs were incubated at 4 °C up to 5 days (Figure S11).

In Vitro Cytotoxicity in the Absence of Radiation. Cytotoxicity of PADO NPs and PADO-NT NPs was examined with H1299 cells, which are a human NSCLC cell line and NTSR1-positive. We first tested PADO-NT NPs made of PADO-MPEG and PADO-PEG-NT at different molar ratios (2:1, 5:1, and 10:1). The ATP viability assay found that PADO-NT NPs made of 2:1 PADO-MPEG and PADO-PEG-NT are the most potent on a per DOX basis (Figure S12). Hence, this formulation was selected for further tests. PADO-NT NPs more efficiently reduced cell viability than PADO NPs, and the difference was more prominent when the DOX concentration was above 50  $\mu$ g/mL (Figure 4A). The enhanced toxicity was attributed to the nanoparticles' ability to traffic DOX across the plasma membrane, more so when they were coupled with NTS<sub>mut</sub>. Interestingly, the difference in

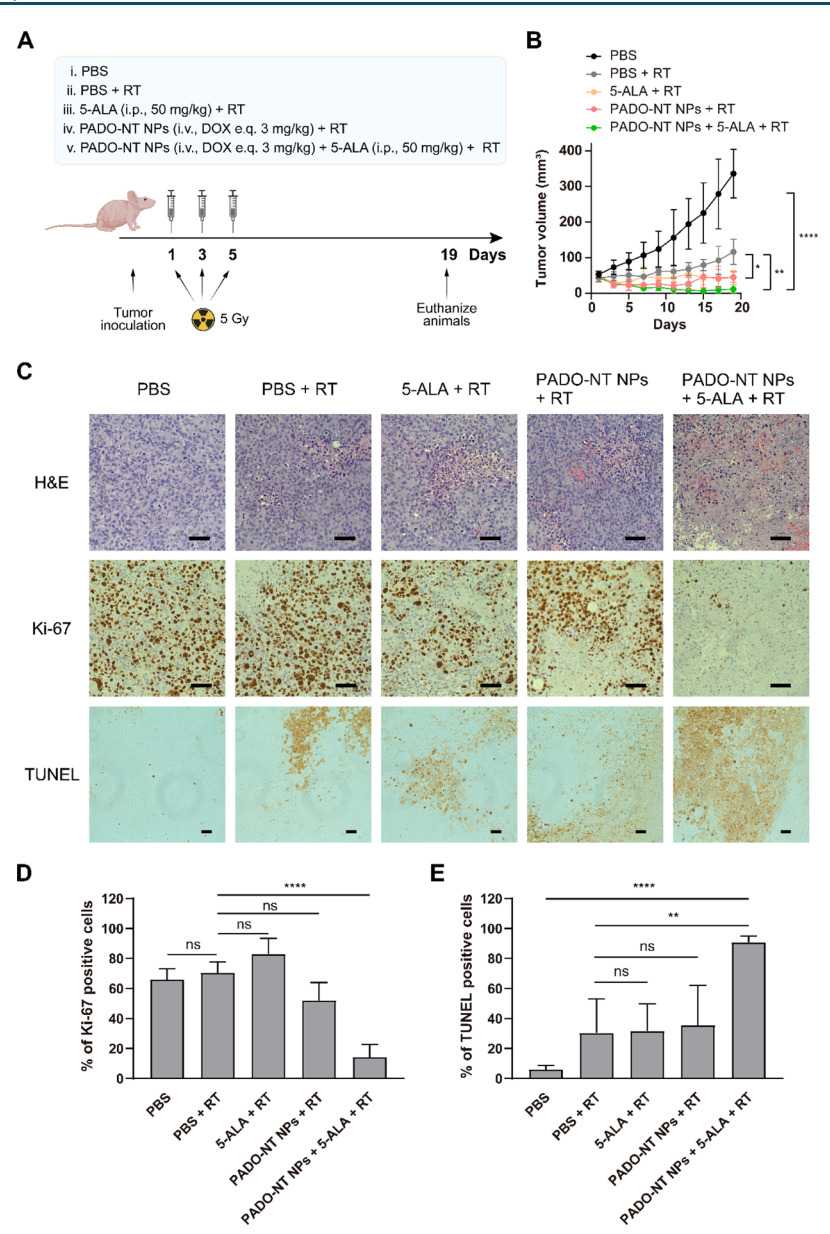


**Figure 6.** Evaluating radiation sensitizing effects *in vivo*. (A) Schematic illustration of the treatment plan. H1299 cells  $(1 \times 10^6)$  were inoculated into nude mice. For the combination treatment group, animals received i.v. injection of PADO-NT NPs (DOX e.q. 3 mg/kg) and i.p. injection of S-ALA (50 mg/kg). Radiation (320 KV, 5 Gy) was applied to tumors after 3 h. Two more treatments were applied on days 3 and 5 (PADO-NT NPs + 5-ALA + RT; n = 5). For comparison, PADO-NT NPs + RT, 5-ALA + RT, PBS + RT, and PBS were also tested (n = 5). All mice were euthanized on day 19. (B) Tumor growth curves, measurement by a caliper using the equation length × width × width × 1/2. (C) H&E (upper), Ki-67(middle), and TUNEL (lower) staining of tumors from all groups. Scale bars, 100  $\mu$ m. (D) Percentage of Ki-67-positive cells, analyzed by ImageJ on the basis of the staining results. (E) Percentage of TUNEL-positive cells. \*p < 0.05; \*\*p < 0.01; \*\*\*\*p < 0.0001; ns, no significant difference.

cytotoxicity was less remarkable at 48 h (Figure S13). This is probably because DOX had been largely released from both particles after 2 days.

We also evaluated cancer cell targeting *in vitro* (Figure 4B). Briefly, we incubated PADO NPs or PADO-NT NPs *in vitro* with H1299 cells and measured DOX fluorescence intensity. For comparison, we treated cells with PADO-NT NPs and sodium azide, a phagocytosis inhibitor. Cells treated with PADO-NT NPs showed much higher DOX intensity than those treated with PADO NPs (p = 0.0006), which is attributed to NTS<sub>mut</sub>-mediated cell uptake. Sodium azide caused a significant decrease in DOX uptake (p = 0.0308), supporting nanoparticle uptake through endocytosis. Note that

sodium azide did not completely block DOX uptake, suggesting that some DOX may have been released from nanoparticles and enter cells on its own.

Evaluating Radiation Sensitizing Effects In Vitro. We first assessed the impact of the 5-ALA on mitochondria (Figure 5A). Accumulation of PpIX plateaued after cancer cells were incubated with 5-ALA for 3 h. Therefore, 3 h was chosen as the drug-radiation interval. While RT alone minimally affected the mitochondria membrane potential ( $\Delta\Psi_{\rm m}$ ), adding 5-ALA to the regimen caused a significant drop of  $\Delta\Psi_{\rm m}$ . This is attributed to the ability of PpIX to boost RT-induced ROS, which is focused on mitochondria. Similar results were observed with other cancer cells.  $^{20,33,34}$  We tested 5-ALA at

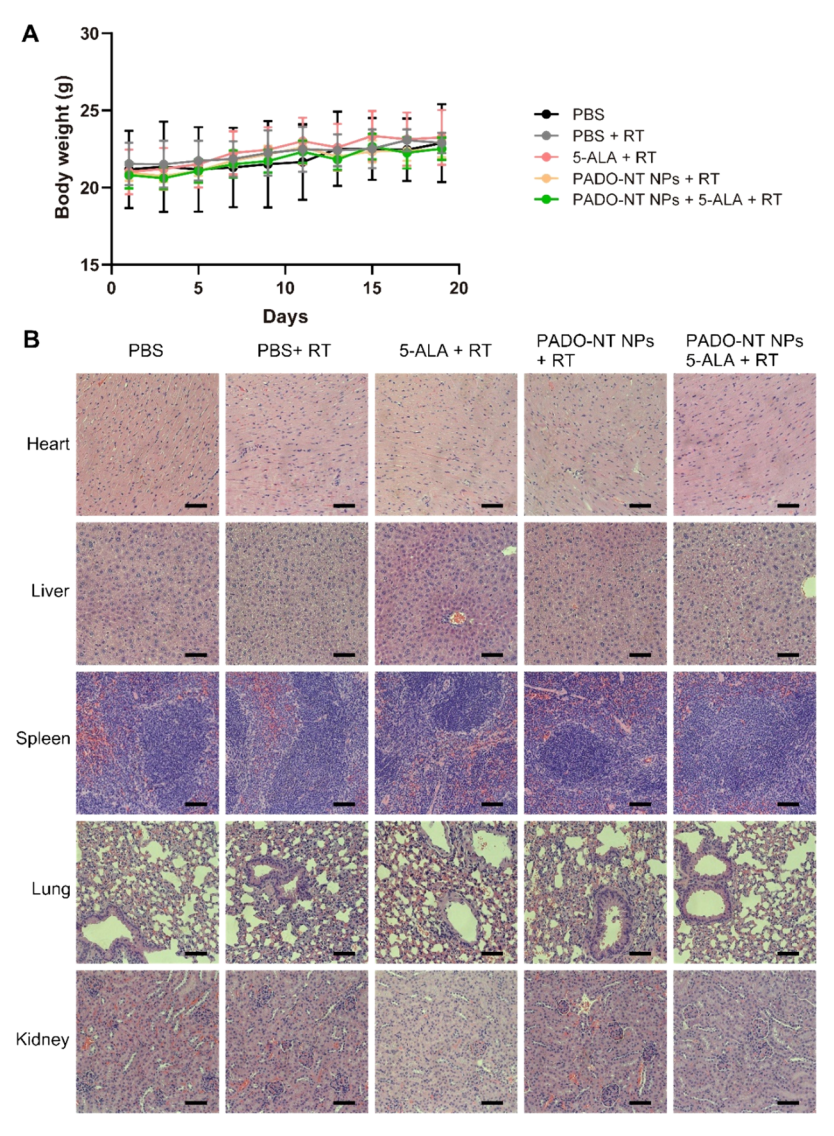


Figure 7. Evaluating toxicity of the combination treatment *in vivo*. (A) Body weight curves of all treatment groups. No significant body weight loss was observed. (B) H&E staining of major organ tissues, including the heart, liver, spleen, lung, and kidney. No pathological changes were observed. Scale bars, 100 µm.

1 mM. Previous studies showed that 5-ALA at this dose is non-toxic to cells, <sup>32,35</sup> which we confirmed (Figure S14).

We next examined the radiosensitizing effects when combining PADO-NT NPs and 5-ALA. We incubated H1299 cells with 5-ALA (1 mM) along with PADO-NT NPs (50  $\mu$ g/mL) for 3 h prior to radiation (5 Gy; Figure 5B). Without radiation, neither PADO-NT NPs, PADO NPs, nor 5-ALA was significantly toxic at the tested concentrations (Figure 4 and Figure S14). Relative to RT alone, cell SOD activity increased in cells treated with 5-ALA + RT or PADO-NT NPs + RT, but the increase was insignificant (p = 0.9689and 0.0968, respectively). Combing 5-ALA and PADO-NT NPs, on the other hand, led to a marked increase in SOD activity, suggesting enhanced oxidative stress. Note that, in addition to RT and 5-ALA, DOX may also contribute to elevated ROS.36-38 We also measured ROS levels with aminophenyl fluorescein (APF), a radical sensor (Figure 5C). The combination of PADO-NT NPs and 5-ALA significantly enhanced RT-induced radicals (p = 0.0144), which is consistent with the SOD results.

We also examined whether the treatment enhanced double-strand breaks by flow cytometry (Figure 5D and Figure S15). Compared to RT alone, positively stained anti- $\gamma$ H2AX cells markedly increased when cells were treated with 5-ALA + RT, which is consistent with the SOD results. PADO-NT NPs + RT also enhanced DNA damage relative to RT alone, which is attributed to DOX-induced DNA intercalation and inhibition of the topoisomerase II complexes. The most prominent double-strand breaks were found in cells treated with a combination of PADO-NT NPs and 5-ALA, presumably due to their complementary mechanisms in radiosensitization.

Last, we investigated how the combination affects viability of irradiated cells. This was examined by the ATP bioluminescence assay, also with H1299 cells (Figure 5E). In accord with the SOD results, 5-ALA alone enhanced RT-induced cytotoxicity, but the decrease was insignificant (p=0.2459). As a comparison, PADO-NT NPs plus 5-ALA caused a dramatic decrease in viability relative to RT alone. Of note, PADO-NPs induced a less prominent radiosensitizing effect than PADO-NT NPs (p<0.05), underscoring the benefits of NTS<sub>mut</sub> in delivery. Overall, our *in vitro* experiments confirm

that 5-ALA can synergize with PADO-NT NPs to increase cancer cells' sensitivity to RT.

Evaluating Radiation Sensitizing Effects In Vivo. In vivo studies were performed in a H1299 xenograft model. Before efficacy studies, we intravenously (i.v.) administered PADO-NT NPs or PADO NPs into H1299 tumor bearing mice and evaluated their distribution in tumors and major organs (Figure S16). Our results confirmed increased tumor accumulation of PADO-NT NPs relative to PADO NPs. Treatment plans are illustrated in Figure 6A. Briefly, when tumor volume reached 50 mm<sup>3</sup>, animals were administered with 5-ALA (intraperitoneally or i.p., 50 mg/kg) and PADO-NT NPs (i.v., equivalent to 3 mg of DOX per kg). Radiation was delivered to the tumor area (320 KV, 5 Gy) after 3 h, with the rest of the animal body lead-shielded (day 1). Two more treatments were applied on days 3 and 5. For comparison, carrier only (PBS), carrier plus radiation therapy (PBS + RT), 5-ALA or PADO-NT NPs alone plus radiation (5-ALA + RT and PADO-NT NPs + RT), and a combination of PADO-NT NPs and 5-ALA (PADO-NT NPs + 5-ALA + RT) were tested. All animals were euthanized on day 19.

PBS + RT only led to moderate tumor suppression compared to the PBS control (Figure 6B). Either 5-ALA + RT or PADO-NT NPs + RT significantly enhanced tumor suppression relative to RT alone (p = 0.0369 and 0.0420, respectively). Their combination led to the most prominent radiosensitizing effects; the improvement was significant relative to either 5-ALA + RT or PADO-NT NPs + RT. Specifically, the tumor suppression rate was 96.6% for the PADO-NT NPs + 5-ALA + RT group, compared to 65.4, 86.6, and 87.0%, respectively, for the PBS + RT, PADO-NT NPs + RT, and 5-ALA + RT groups. In particular, all animals in the PADO-NT NPs + 5-ALA + RT group experienced tumor regression; 40% of the mice underwent complete tumor eradication by day 19.

Tumor and healthy tissues were harvested after animal euthanasia for histopathology (Figure 6C). Compared to control groups, tumors treated with PADO-NT NPs + 5-ALA + RT manifest a reduced cell density (Figure 6C, upper) and a decreased level of positive staining for Ki-67 (Figure 6C, middle and Figure 6D) (p < 0.0001). The radiosensitizing effects were also validated with TUNEL staining (Figure 6C, lower), finding an increased level of apoptosis in tumors from the PADO-NT NPs + 5-ALA + RT group (p = 0.0018; Figure 6C,E). Meanwhile, no acute toxicity or significant body weight drop was observed throughout the experiment (Figure 7A). H&E staining found no signs of side effects in major organs (Figure 7B). In particular, there is no significant cardiotoxicity, which is a major dose-limiting factor for DOX treatment. Overall, our in vivo experiment confirms that the combination of 5-ALA and PADO-NT NPs can enhance RT without inducing additional toxicity.

## CONCLUSIONS

In this work, we investigated a new radiosensitizing approach involving systematically administrated 5-ALA and DOX-conjugated nanoparticles. Rather than injecting the two therapeutics together in a single formulation, we administer them separately, exploiting the tumor targeting ability of 5-ALA and PADO-NT NPs. This strategy avoids the use of a complex hybrid nanoparticle, which is associated with issues such as difficulties to scale up manufacturing, varied physiochemical properties between payloads, and differences

in effective therapeutic doses among active ingredients. 5-ALA is an FDA-approved agent and can be taken orally or topically by patients. PADO-NT NPs target NTSR1, which is overexpressed in the majority of lung cancer patients, <sup>21</sup> and its upregulation is strongly correlated with reduced disease-free survival and overall survival. <sup>21</sup> DOX release is mediated by the cleavage of hydrazone that is facilitated in the acidic tumor microenvironment. Combining them, these properties for selective radiosensitization have not been explored and are clinically relevant.

We choose PSI as the polymer backbone for at least the following reasons. First, PSI is biocompatible, biodegradable, and non-immunogenic.  $^{40-42}$  PSI is polymerized from L-aspartic acid, a natural amino acid. After ring-opening reaction with side chains containing amine groups, the resulting polyaspartamide degrades to non-toxic byproducts. Second, PSI can be easily coupled with versatile graft chains and therapeutics.  $^{43-51}$  The facile coupling chemistry makes the polymer an ideal platform to construct nanoparticles incorporated with targeting, imaging, and therapeutic functions.

While the results are promising, measures can be taken to improve the efficacy of the approach. For instance, it is possible to optimize the drug-radiation interval and increasing 5-ALA and/or PADO-NT NP dosages. It is also feasible to extend the chemistry to load other chemotherapeutics such as carboplatin, 5-fluorouracil, and paclitaxel or a combination of them. These possibilities will be pursued in future investigations.

## METHODS

Materials. L-Aspartic acid (98%), mesitylene (98%), sulfolane (99%), phosphoric acid (crystallized, 99.0%), octadecylamine (99%), triethylamine (99%), and hydrazine monohydrate (64-65%) were purchased from Sigma-Aldrich (St. Louis, MO, USA). Milli-Q Water (H<sub>2</sub>O, 18.2 MΩ·cm@25 °C) was obtained from Millipore Milli-Q water purification system. MPEG-NH<sub>2</sub> (Mw = 5000, 95%) and MAL-PEG-NH<sub>2</sub> (Mw = 5000, 95%) were obtained from Biopharma PEG (Biochempeg) Scientific Inc. (Watertown, MA, USA). Doxorubicin hydrochloride (95%) was supplied by TCI America (Portland, OR, USA). Trifluoroacetic acid (99%) and N,N-dimethylformamide (DMF, anhydrous, 99.9%) were purchased from Alfa Aesar (Haverhill, MA, USA). Cys-NTS<sub>mut</sub> peptide (sequence: Ac-Cys-Pro-(NMe-Arg)-Arg-Pro-Tyr-Tle-Leu, modified from a previously reported sequence 22,52 by replacing lysine with cysteine) was purchased from CSBio (Menlo Park, CA, USA).

**Synthesis of NT-PEG-NH<sub>2</sub>.** A solution of Cys-NTS<sub>mut</sub> peptide (45 mg, 42  $\mu$ mol) in DMSO (3 mL) and a solution of Mal-PEG-NH<sub>2</sub> (105 mg, 21  $\mu$ mol) in DMF (6 mL) were mixed and stirred under the atmosphere of N<sub>2</sub> at room temperature for 48 h. The reaction mixture was diluted by mixing with 30 mL of DI water. Excessive Cys-NTS<sub>mut</sub> peptide was removed by ultracentrifugation using a centrifugal filter device (Amicon, MWCO: 3000 Da) and freeze-dried to give a white powder (120 mg). The filtrate was collected, and the reaction efficiency was analyzed by HPLC (HPLC conditions are detailed in the Supporting Information).

**Synthesis of PSI.** A suspension of L-aspartic acid (10 g, 75.13 mmol) and phosphoric acid (0.74 g, 7.51 mmol) in a mixed solvent of mesitylene (22.4 mL) and sulfolane (10.0 mL) was refluxed at 170  $^{\circ}$ C under a  $N_2$  atmosphere for 6 h. Water formed in the reaction mixture was eliminated using a

Dean—Stark trap with a reflux condenser. The reaction system was cooled down to room temperature and filtered. The residue was collected and washed successively with methanol (250 mL) and water until it was neutral. The residue was dried and then redissolved in DMF (10 mL) and filtered. The filtrate was dropwise added into methanol (600 mL) under vigorous stirring. Solid from the reaction was collected by filtration and washed with methanol (200 mL). The white powder (4.7 g, 64% yield) was obtained after dried at 85 °C under reduced pressure.

Synthesis of Grafted Copolymer PADO-MPEG and PADO-PEG-NT. To a solution of PSI (15 mg, 0.15 mmol repeating units) in DMF (0.5 mL), octadecylamine (8.3 mg, 0.03 mmol) was added at 40 °C. After 48 h, a solution of MPEG5000-NH<sub>2</sub> (232 mg, 0.046 mmol) in DMF (1 mL) was added. The reaction continued for another 48 h. Then, the reaction mixture was diluted to 3 mL with DMF. Hydrazine monohydrate (0.15 mL, 3.09 mmol) in DMF (1 mL) was slowly added at room temperature. The reaction was conducted for 6 h, and the product PAO-MPEG was purified using a dialysis membrane (Spectrum, MWCO: 10 kDa) against DI water for 3 days followed by lyophilization.

PAO-MPEG (100 mg) was dissolved in methanol (10 mL). DOX·HCl (35 mg) was suspended in the solution followed by the addition of TFA (0.01 mL). The reaction was conducted under a  $\rm N_2$  atmosphere in the dark at room temperature for 3 days. TEA (0.5 mL) was added and stirred for 1 h. Then, the solvent was removed under vacuum. Excessive DOX and salts were eliminated by ultracentrifugation using a centrifugal filter device (Amicon, MWCO: 10 kDa). The filtrate was lyophilized, yielding PADO-MPEG.

 $\rm NTS_{mut}\text{-}functionalized}$  copolymer PADO-PEG-NT was prepared following the same protocol. The theoretical DOX LC% was calculated based on the following equation:

DOX LC% = 0.5 Mw of DOX/(Mw of repeating units + 0.2 Mw of octadecylamine + 0.3 Mw of PEG + 0.5 Mw of DOX)  $\times$  100%

Preparation of PADO NPs and PADO-NT NPs. To prepare PADO NPs, 200  $\mu$ L of PBS was added to 1 mg of lyophilized PADO-MPEG followed by 1 min sonication to obtain a homogeneous nanoparticle suspension. To prepare PADO-NT NPs, a mixture of PADO-MPEG/PADO-PEG-NT (molar ratios of 2:1, 5:1, and 10:1) was dissolved in PBS followed by 1 min sonication. Cytotoxicity of the PADO-NT NPs with different ratios was evaluated and compared, see Figure S12.

Critical Aggregation Concentration Measurement. PBS (200  $\mu$ L) was mixed with 1 mg of lyophilized PADO-MPEG or PADO-NT followed by 1 min sonication to obtain solutions of PADO NPs or PADO-NT NPs. A series of diluted solutions (from 125 to 1.953125  $\mu$ g/mL) were subjected to DLS analysis on a Malvern Zetasizer Nano ZS system, and the count rates (kcps) were recorded.

Characterizations of PADO NPs and PADO-NT NPs. Hydrodynamic sizes and zeta potentials of nanoparticles were analyzed on a Malvern Zetasizer Nano ZS system. Transmission electron microscopy (TEM) and scanning electron microscopy (SEM) were performed on STEM – Hitachi SU9000EA, operated at 30 kV, 1  $\mu$ A.

**Colloidal Stability and Drug Release.** PADO NPs were dispersed in PBS (pH = 7.4) and stored at 4 °C. At different time points (0, 1, 2, 3, 5, and 7 days), the size of the nanoparticle was measured by DLS (Malvern Zetasizer Nano

ZS system). To study DOX release, freshly prepared PADO NPs were dispersed in 200  $\mu$ L of PBS (pH = 6.5 or 7.4) or sodium acetate buffer (pH = 5.0). The nanoparticle solution was then transferred into a Slide-A-Lyzer Mini Dialysis Device (MWCO: 3.5 K, Cat #69550), which was placed into an Eppendorf tube containing 2 mL of the solvent. The tube was kept on a shaker (60 rpm) at 37 °C. At different time points (1, 2, 3, 6, 9, 12, 18, 24, 36, 48, and 72 h), 100  $\mu$ L of solution was aspirated from the Eppendorf tube for measurement of the DOX concentration. Fresh buffer (100  $\mu$ L) was added to the tube to maintain the solution volume. The DOX concentration was measured by analyzing its 480 nm absorbance on a microplate reader (Synergy Mx, BioTek) and comparing to a calibration curve.

**Cell Culturing.** H1299 cells were cultured in RPMI-1640 (Corning, 10-040-CV) that was supplemented with 10% fetal bovine serum (FBS) and 100 units/mL penicillin and streptomycin (Gibco, Cat #15070063). Cells were maintained in an incubator at 37  $^{\circ}$ C with a humidified 5%  $CO_2$  atmosphere.

Cytotoxicity. An ATPlite-1 step luminescence ATP detection assay kit (PerkinElmer, Cat #6016731) was used to measure cell cytotoxicity, following the manufacturer's protocol. Briefly, H1299 cells were seeded into a 96-well white plate (Costar, Cat #3610) at a density of 5000 cells per well and incubated overnight. The cells were then treated with PADO NPs, PADO-NT NPs, or DOX at an e.q. dose of DOX ranging from 1.5625 to 100  $\mu$ g/mL. After 24 h of incubation, the supernatant was removed followed by the addition of 50  $\mu$ L of PBS and 50  $\mu$ L of ATP kit solution. The plate was incubated in the dark for 10 min before measuring luminescence signals on a microplate reader (Synergy Mx, BioTek). To study the radiation sensitizing effects of 5-ALA, PADO NPs, and PADO-NT NPs, cells were treated with PBS, PBS + RT, 5-ALA (1 mM) + RT, PADO NPs + 5-ALA (1 mM) + RT, or PADO-NT NPs + 5-ALA (1 mM) + RT. For the PBS and PBS + RT groups, PBS was added instead of nanoparticles. PADO NPs and PADO-NT NPs were added at an equivalent DOX concentration of 50 µg/mL. After 3 h of incubation, 5 Gy radiation was applied to cells. The cells were cultured for another 24 h before measuring their bioluminescence signals.

**Cellular Uptake.** H1299 cells were incubated with PBS, PADO NPs, PADO-NT NPs, or PADO-NT NPs + NaN $_3$  (50 mM). PADO NPs and PADO-NT NPs were added at an e.q. DOX concentration of 50  $\mu$ g/mL. After 2 h, cells were collected by a cell lifter and washed once with PBS. Cells were then resuspended in staining buffer, stained with DAPI (Thermo Fisher Scientific), and fixed with a mixture of IC fixation buffer (Invitrogen, Cat #00-8222-49)/stain buffer (1:1) for 30 min. Trypan blue solution was added to quench fluorescence from nanoparticles non-specifically associated to the cell membrane. Flow cytometry was used to analyze the mean fluorescence intensity from the intercellular DOX.

**Mitochondrial Damage.**  $\Delta\Psi_m$  change was measured using a MitoPT JC-1 assay (ImmunoChemistry, Cat #924). Briefly,  $1\times10^6$  H1299 cells were seeded onto a six-well plate and incubated overnight. Cells were then treated with 5-ALA (1 mM) or PBS for 3 h followed by 5 Gy radiation. Twenty-four hours after the radiation, cells were processed following a manufacturer-provided protocol. Carbonyl cyanide 3-chlorophenylhydrazone (CCCP) was tested as a positive control.

**Superoxide Dismutase (SOD) Activity.** A superoxide dismutase assay kit (Cayman, Cat #706002) was used for the measurement. Specifically,  $1 \times 10^6$  H1299 cells were seeded onto a six-well plate and incubated overnight. Cells were then treated under different conditions: PBS, PBS + RT, 5-ALA (1 mM) + RT, PADO-NT NPs + RT, and PADO-NT NPs + 5-ALA + RT for 3 h followed by 5 Gy radiation. For PBS and PBS + RT groups, PBS was added instead of nanoparticle solution. For PADO NPs and PADO-NT NPs, the DOX e.q. concentration was  $50 \, \mu \text{g/mL}$ . One hour after the radiation, the cells were processed and the SOD activity was measured following the vendor's protocol.

Reactive Oxygen Species (ROS) Level. Aminophenyl fluorescein (APF) purchased from Thermo Fisher Scientific (Cat #A36003) was used as a hydroxy radical indicator. Specifically, 5000 H1299 cells were seeded onto a 96-well plate 1 day before the experiment. Cells were then treated with PBS, 5-ALA (1 mM), PADO-NT NPs, or PADO-NT NPs + 5-ALA. PADO NPs and PADO-NT NPs were added at a DOX e.q. concentration of 50  $\mu$ g/mL. After 2.5 h, APF at the working concentration (following the vendor's protocol) was added and incubated with cells for 3 h. Fluorescence intensity at ex/em: 490/515 nm was measured before and immediately after radiation (5 Gy) was applied. The ratio of APF fluorescence intensity after and before radiation was used to measure ROS changes.

 $\gamma$ H2AX Staining. Briefly,  $1 \times 10^6$  H1299 cells were seeded onto a six-well plate 1 day before the experiment. Cells were then treated under different conditions: PBS, PBS + RT, 5-ALA (1 mM) + RT, PADO-NT NPs + RT, and PADO-NT NPs + 5-ALA + RT for 3 h followed by 5 Gy radiation. For PBS and PBS + RT groups, PBS was added instead of nanoparticle solution. For PADO NPs and PADO-NT NPs, the DOX e.q. concentration was 50  $\mu$ g/mL. Four hours after the radiation, cells were collected by a cell lifter and washed once with PBS. Cells were then resuspended in staining buffer, stained with DAPI (Thermo Fisher Scientific), and fixed with a mixture of IC fixation buffer (Invitrogen, Cat #00-8222-49)/ stain buffer (1:1) for 30 min. Cells were then permeabilized in diluted permeabilization buffer (Invitrogen, Cat #00-8333-56) for 30 min followed by blocking with 1% goat serum for 1 h. For γH2AX staining, cells were then stained with Alexa Fluor 647 anti-H2A.X (BioLegend, Cat #613408) for 1 h. After washing, flow cytometry was performed to analyze the cells.

**Biodistribution.** Female nude mice (purchased from Charles River) bearing subcutaneously inoculated H1299 tumors were used. When tumor size reached 100 mm<sup>3</sup>, the animals were i.v. administered with PADO NPs or PADO-NT NPs (n=3) at an equivalent DOX dose of 10 mg/kg. After 3 h, the mice were euthanized. Tumors as well as major organs including the heart, liver, spleen, lung, and kidney were collected and weighed. After homogenization in PBS, the supernatant was collected by centrifugation and the DOX concentration was quantified by measuring fluorescence intensity (ex/em: 470/595 nm) and comparing with a calibration curve.

*In Vivo* Radiation Therapy. All animal experiments were performed under the guidelines for Care and Use of Laboratory Animals of the University of Georgia and following protocols approved by the Institutional Animal Care and Use Committee (IACUC) of the University of Georgia. Therapy was carried out on female nude mice (purchased from Charles River) bearing H1299 subcutaneous tumors. H1299 cells (1 ×

10<sup>6</sup>) were inoculated into the right flank of a mouse. When tumor size reaches 50 mm<sup>3</sup> (day 1), mice were randomly divided into five groups: PBS, PBS + RT, 5-ALA + RT, PADO-NT NPs + RT, and PADO-NT NPs + 5-ALA + RT. For PBS and PBS + RT groups, PBS was used instead of nanoparticle solution. PADO-NT NPs were intravenously injected with a DOX e.q. concentration of 3 mg/kg. 5-ALA was intraperitoneally injected at a dose of 50 mg/kg. Radiation (5 Gy) to the tumor on mice was delivered 3 h after 5-ALA and nanoparticle injection. The same treatments were given on days 3 and 5. There were five mice in each group. Tumor size and body weight were measured every 2 days, and tumor volume was calculated by the equation length × width × width × 1/2. Mice were euthanized on day 19. Tumor, heart, liver, spleen, lung, and kidney tissues were collected and sent to a pathology lab for H&E and Ki-67 staining. TUNEL staining (Abcam, Cat #ab206386) was performed on tumor samples following the vendor's protocol. Quantification of Ki-67 and TUNEL staining was performed using ImageJ by counting percentage of positively stained cells per higher power field.

**Statistical Analysis.** For the JC-1 assay and cytotoxicity study of PADO NPs and PADO-NT NPs, measurements were performed in quadruplicates. For cytotoxicity studies, measurements were performed in sextuplicates. All other *in vitro* experiments were performed in triplicates. All data were represented as mean  $\pm$  S.D. unless otherwise specified. Graphpad Prism 8 software (Graphpad Software, San Diego, CA) was used for data analysis. Statistical significances between groups were determined by one-way ANOVA with post-hoc Turkey–Kramer comparisons with p value <0.05 considered significantly different.

## ASSOCIATED CONTENT

## Supporting Information

The Supporting Information is available free of charge at https://pubs.acs.org/doi/10.1021/acs.bioconjchem.2c00066.

Figures showing <sup>1</sup>H NMR spectra, HPLC conditions, NP stability, ATP bioluminescence assays, and the flow cytometry gating strategy (PDF)

## AUTHOR INFORMATION

## **Corresponding Authors**

Jin Xie – Department of Chemistry, University of Georgia, Athens, Georgia 30602, United States; oorcid.org/0000-0002-8915-6233; Email: jinxie@uga.edu

Xinglu Huang — State Key Laboratory of Medicinal Chemical Biology, and Key Laboratory of Bioactive Materials, Ministry of Education, College of Life Sciences, Nankai University, Tianjin 300071, China; orcid.org/0000-0002-9378-7425; Email: huangxinglu@nankai.edu.cn

#### **Authors**

Jinghua Han — College of Pharmacy, Tianjin Key Laboratory of Molecular Drug Research, Nankai University, Tianjin 300353, China; orcid.org/0000-0001-9546-8172

Wei Yang – Department of Chemistry, University of Georgia, Athens, Georgia 30602, United States; ⊚ orcid.org/0000-0001-6905-2296

Yuanke Li — State Key Laboratory of Medicinal Chemical Biology, and Key Laboratory of Bioactive Materials, Ministry of Education, College of Life Sciences, Nankai University, Tianjin 300071, China Jianwen Li − Department of Chemistry, University of Georgia, Athens, Georgia 30602, United States; ocid.org/0000-0002-3936-937X

Fangchao Jiang — Department of Chemistry, University of Georgia, Athens, Georgia 30602, United States;
orcid.org/0000-0002-3679-4012

Complete contact information is available at: https://pubs.acs.org/10.1021/acs.bioconjchem.2c00066

#### **Author Contributions**

All authors have given approval to the final version of the manuscript.

#### **Notes**

The authors declare no competing financial interest.

### ACKNOWLEDGMENTS

This work was supported by the National Natural Science Foundation of China (91959129). We also thank the support from the Georgia Research Alliance. Figure <sup>1</sup>, the TOC figure, and Figure <sup>6</sup>A were created at BioRender.com.

### REFERENCES

- (1) Sung, H.; Ferlay, J.; Siegel, R. L.; Laversanne, M.; Soerjomataram, I.; Jemal, A.; Bray, F. Global Cancer Statistics 2020: GLOBOCAN Estimates of Incidence and Mortality Worldwide for 36 Cancers in 185 Countries. *CA: A Cancer Journal for Clinicians* 2021, 71, 209–249.
- (2) Molina, J. R.; Yang, P.; Cassivi, S. D.; Schild, S. E.; Adjei, A. A. Non-Small Cell Lung Cancer: Epidemiology, Risk Factors, Treatment, and Survivorship. *Mayo Clinic Proceedings* **2008**, *83*, 584–594.
- (3) Howington, J. A.; Blum, M. G.; Chang, A. C.; Balekian, A. A.; Murthy, S. C. Treatment of Stage I and II Non-small Cell Lung Cancer: Diagnosis and Management of Lung Cancer, 3rd ed: American College of Chest Physicians Evidence-Based Clinical Practice Guidelines. *Chest* 2013, 143, e278S—e313S.
- (4) Walters, S.; Maringe, C.; Coleman, M. P.; Peake, M. D.; Butler, J.; Young, N.; Bergström, S.; Hanna, L.; Jakobsen, E.; Kölbeck, K.; et al. Lung cancer survival and stage at diagnosis in Australia, Canada, Denmark, Norway, Sweden and the UK: a population-based study, 2004-2007. *Thorax* **2013**, *68*, 551–564.
- (5) Wang, J. S.; Wang, H. J.; Qian, H. L. Biological effects of radiation on cancer cells. *Mil Med Res* 2018, 5, 20.
- (6) Lomax, M. E.; Folkes, L. K.; O'Neill, P. Biological consequences of radiation-induced DNA damage: relevance to radiotherapy. *Clin Oncol (R Coll Radiol)* **2013**, 25, 578–585.
- (7) Srinivas, U. S.; Tan, B. W. Q.; Vellayappan, B. A.; Jeyasekharan, A. D. ROS and the DNA damage response in cancer. *Redox Biol* **2019**, 25, 101084.
- (8) Dilling, T. J. Radiation Dose in Non Small Cell Lung Cancer: Too Much of a Good Thing? *Int. J. Radiat. Oncol., Biol., Phys.* **2014**, 90, 979–982.
- (9) Skrzypski, M.; Jassem, J. Consolidation systemic treatment after radiochemotherapy for unresectable stage III non-small cell lung cancer. *Cancer Treatment Reviews* **2018**, *66*, 114–121.
- (10) Langer, R. Drug delivery and targeting. *Nature* **1998**, 392, 5–10.
- (11) Luksiene, Z.; Juzenas, P.; Moan, J. Radiosensitization of tumours by porphyrins. *Cancer Lett.* **2006**, 235, 40–47.
- (12) Takahashi, J.; Misawa, M. Characterization of reactive oxygen species generated by protoporphyrin IX under X-ray irradiation. *Radiat. Phys. Chem.* **2009**, *78*, 889–898.
- (13) Wang, Y.; Zhang, H.; Hao, J.; Li, B.; Li, M.; Xiuwen, W. Lung cancer combination therapy: co-delivery of paclitaxel and doxorubicin by nanostructured lipid carriers for synergistic effect. *Drug Delivery* **2016**, 23, 1398–1403.

- (14) Gu, Y.; Li, J.; Li, Y.; Song, L.; Li, D.; Peng, L.; Wan, Y.; Hua, S. Nanomicelles loaded with doxorubicin and curcumin for alleviating multidrug resistance in lung cancer. *Int. J. Nanomed.* **2016**, *Volume 11*, 5757
- (15) Hong, Y.; Che, S.; Hui, B.; Yang, Y.; Wang, X.; Zhang, X.; Qiang, Y.; Ma, H. Lung cancer therapy using doxorubicin and curcumin combination: targeted prodrug based, pH sensitive nanomedicine. *Biomed. Pharmacother.* **2019**, *112*, 108614.
- (16) Cai, X.; Luo, Y.; Zhang, W.; Du, D.; Lin, Y. pH-Sensitive ZnO quantum dots—doxorubicin nanoparticles for lung cancer targeted drug delivery. ACS Appl. Mater. Interfaces 2016, 8, 22442—22450.
- (17) Srivastava, A.; Amreddy, N.; Babu, A.; Panneerselvam, J.; Mehta, M.; Muralidharan, R.; Chen, A.; Zhao, Y. D.; Razaq, M.; Riedinger, N.; Kim, H.; Liu, S.; Wu, S.; Abdel-Mageed, A. B.; Munshi, A.; Ramesh, R. Nanosomes carrying doxorubicin exhibit potent anticancer activity against human lung cancer cells. *Sci. Rep.* **2016**, *6*, 1–15.
- (18) Jurisicova, A.; Lee, H. J.; D'Estaing, S. G.; Tilly, J.; Perez, G. I. Molecular requirements for doxorubicin-mediated death in murine oocytes. *Cell Death & Differentiation* **2006**, *13*, 1466–1474.
- (19) Goto, S.; Ihara, Y.; Urata, Y.; Izumi, S.; Abe, K.; Koji, T.; Kondo, T. Doxorubicin-induced DNA intercalation and scavenging by nuclear glutathione S-transferase  $\pi$ . FASEB J. **2001**, 15, 2702–2714.
- (20) Ueta, K.; Yamamoto, J.; Tanaka, T.; Nakano, Y.; Kitagawa, T.; Nishizawa, S. 5-Aminolevulinic acid enhances mitochondrial stress upon ionizing irradiation exposure and increases delayed production of reactive oxygen species and cell death in glioma cells. *Int J Mol Med* **2017**, *39*, 387–398.
- (21) Alifano, M.; Souazé, F.; Dupouy, S.; Camilleri-Broët, S.; Younes, M.; Ahmed-Zaïd, S.-M.; Takahashi, T.; Cancellieri, A.; Damiani, S.; Boaron, M.; Broët, P.; Miller, L. D.; Gespach, C.; Regnard, J. F.; Forgez, P. Neurotensin receptor 1 determines the outcome of non–small cell lung cancer. *Clinical Cancer Research* **2010**, *16*, 4401–4410.
- (22) Deng, H.; Wang, H.; Zhang, H.; Wang, M.; Giglio, B.; Ma, X.; Jiang, G.; Yuan, H.; Wu, Z.; Li, Z. Imaging Neurotensin Receptor in Prostate Cancer With <sup>64</sup>Cu-Labeled Neurotensin Analogs. *Mol. Imaging* **2017**, *16*, 1536012117711369.
- (23) Bae, Y.; Kataoka, K. Intelligent polymeric micelles from functional poly(ethylene glycol)-poly(amino acid) block copolymers. *Adv. Drug Delivery Rev.* **2009**, *61*, 768–784.
- (24) Prabaharan, M.; Grailer, J. J.; Pilla, S.; Steeber, D. A.; Gong, S. Amphiphilic multi-arm-block copolymer conjugated with doxorubicin via pH-sensitive hydrazone bond for tumor-targeted drug delivery. *Biomaterials* **2009**, *30*, 5757–5766.
- (25) Jiang, T.; Li, Y.-M.; Lv, Y.; Cheng, Y.-J.; He, F.; Zhuo, R.-X. Amphiphilic polycarbonate conjugates of doxorubicin with pH-sensitive hydrazone linker for controlled release. *Colloids Surf., B* **2013**, *111*, 542–548.
- (26) Miyake, M.; Ishii, M.; Kawashima, K.; Kodama, T.; Sugano, K.; Fujimoto, K.; Hirao, Y. siRNA-mediated knockdown of the heme synthesis and degradation pathways: modulation of treatment effect of 5-aminolevulinic acid-based photodynamic therapy in urothelial cancer cell lines. *Photochem. Photobiol.* **2009**, 85, 1020–1027.
- (27) Amo, T.; Kawanishi, N.; Uchida, M.; Fujita, H.; Oyanagi, E.; Utsumi, T.; Ogino, T.; Inoue, K.; Shuin, T.; Utsumi, K.; Sasaki, J. Mechanism of cell death by 5-aminolevulinic acid-based photodynamic action and its enhancement by ferrochelatase inhibitors in human histiocytic lymphoma cell line U937. *Cell Biochem. Funct.: Cellular biochem. modulation act. agents dis.* **2009**, *27*, 503–515.
- (28) Yamamoto, J.; Ogura, S.-i.; Tanaka, T.; Kitagawa, T.; Nakano, Y.; Saito, T.; Takahashi, M.; Akiba, D.; Nishizawa, S. Radiosensitizing effect of 5-aminolevulinic acid-induced protoporphyrin IX in glioma cells in vitro. *Oncol. Rep.* **2012**, *27*, 1748–1752.
- (29) Yamamoto, J.; Ogura, S.-i.; Shimajiri, S.; Nakano, Y.; Akiba, D.; Kitagawa, T.; Ueta, K.; Tanaka, T.; Nishizawa, S. 5-Aminolevulinic acid-induced protoporphyrin IX with multi-dose ionizing irradiation enhances host antitumor response and strongly inhibits tumor growth in experimental glioma in vivo. *Mol. Med. Rep.* **2015**, *11*, 1813–1819.

- (30) Takahashi, J.; Murakami, M.; Mori, T.; Iwahashi, H. Verification of radiodynamic therapy by medical linear accelerator using a mouse melanoma tumor model. *Sci. Rep.* **2018**, *8*, 1–9.
- (31) Tomida, M.; Nakato, T.; Matsunami, S.; Kakuchi, T. Convenient synthesis of high molecular weight poly(succinimide) by acid-catalysed polycondensation of L-aspartic acid. *Polymer* 1997, 38, 4733–4736.
- (32) Predina, J. D.; Runge, J.; Newton, A.; Mison, M.; Xia, L.; Corbett, C.; Shin, M.; Sulyok, L. F.; Durham, A.; Nie, S.; Singhal, S.; Holt, D. Evaluation of aminolevulinic acid-derived tumor fluorescence yields disparate results in murine and spontaneous large animal models of lung cancer. *Sci. Rep.* **2019**, *9*, 1–10.
- (33) Sugiyama, Y.; Hagiya, Y.; Nakajima, M.; Ishizuka, M.; Tanaka, T.; Ogura, S.-I. The heme precursor 5-aminolevulinic acid disrupts the Warburg effect in tumor cells and induces caspase-dependent apoptosis. *Oncol. Rep.* **2014**, *31*, 1282–1286.
- (34) Kaneko, T.; Tominaga, M.; Kouzaki, R.; Hanyu, A.; Ueshima, K.; Yamada, H.; Suga, M.; Yamashita, T.; Okimoto, T.; Uto, Y. Radiosensitizing effect of 5-aminolevulinic acid and protoporphyrin IX on carbon-ion beam irradiation. *Anticancer Res.* **2018**, 38, 4313–4317.
- (35) Kitagawa, T.; Yamamoto, J.; Tanaka, T.; Nakano, Y.; Akiba, D.; Ueta, K.; Nishizawa, S. 5-Aminolevulinic acid strongly enhances delayed intracellular production of reactive oxygen species (ROS) generated by ionizing irradiation: Quantitative analyses and visualization of intracellular ROS production in glioma cells in vitro. *Oncol. Rep.* 2015, 33, 583–590.
- (36) Kluza, J.; Marchetti, P.; Gallego, M.-A.; Lancel, S.; Fournier, C.; Loyens, A.; Beauvillain, J.-C.; Bailly, C. Mitochondrial proliferation during apoptosis induced by anticancer agents: effects of doxorubicin and mitoxantrone on cancer and cardiac cells. *Oncogene* **2004**, 23, 7018–7030.
- (37) Thorn, C. F.; Oshiro, C.; Marsh, S.; Hernandez-Boussard, T.; McLeod, H.; Klein, T. E.; Altman, R. B. Doxorubicin pathways: pharmacodynamics and adverse effects. *Pharmacogenet. Genomics* **2011**, *21*, 440–446.
- (38) Gewirtz, D. A. A critical evaluation of the mechanisms of action proposed for the antitumor effects of the anthracycline antibiotics adriamycin and daunorubicin. *Biochem. Pharmacol.* **1999**, *57*, 727–741.
- (39) Pommier, Y.; Leo, E.; Zhang, H.; Marchand, C. DNA Topoisomerases and Their Poisoning by Anticancer and Antibacterial Drugs. *Chem. Biol.* **2010**, *17*, 421–433.
- (40) Wang, Y.; Wang, Y.; Wu, G.; Fan, Y.; Ma, J. pH-Responsive Self-Assembly and conformational transition of partially propylesterified poly( $\alpha,\beta$ -1-aspartic acid) as amphiphilic biodegradable polyanion. *Colloids Surf., B* **2009**, *68*, 13–19.
- (41) Carfi Pavia, F.; La Carrubba, V.; Brucato, V.; Palumbo, F. S.; Giammona, G. Synthesis, characterization and foaming of PHEA–PLLA, a new graft copolymer for biomedical engineering. *Mater. Sci. Eng.*, C 2014, 41, 301–308.
- (42) Adelnia, H.; Tran, H. D. N.; Little, P. J.; Blakey, I.; Ta, H. T. Poly(aspartic acid) in Biomedical Applications: From Polymerization, Modification, Properties, Degradation, and Biocompatibility to Applications. ACS Biomater. Sci. Eng. 2021, 7, 2083–2105.
- (43) Aderibigbe, B. A.; Ray, S. S. Preparation, characterization and in vitro release kinetics of polyaspartamide-based conjugates containing antimalarial and anticancer agents for combination therapy. *Journal of Drug Delivery Science and Technology* **2016**, *36*, 34–45.
- (44) Mukaya, H. E.; van Zyl, R. L.; van Vuuren, N. J.; Mbianda, X. Y. Synthesis and characterization of water-soluble polyaspartamides containing platinum(II) complex and bisphosphonate as potential antimalarial drug. *Polym. Bull.* **2017**, *74*, 3161–3178.
- (45) Di Meo, C.; Cilurzo, F.; Licciardi, M.; Scialabba, C.; Sabia, R.; Paolino, D.; Capitani, D.; Fresta, M.; Giammona, G.; Villani, C.; et al. Polyaspartamide-Doxorubicin Conjugate as Potential Prodrug for Anticancer Therapy. *Pharm. Res.* **2015**, *32*, 1557–1569.
- (46) Aderibigbe, B. A.; Jacques, K. D.; Neuse, E. W. Polymeric Conjugates of Selected Aminoquinoline Derivatives as Potential Drug

- Adjuvants in Cancer Chemotherapy. J. Inorg. Organomet. Polym. Mater. 2011, 21, 336-345.
- (47) Mauro, N.; Schillaci, D.; Varvarà, P.; Cusimano, M. G.; Geraci, D. M.; Giuffrè, M.; Cavallaro, G.; Maida, C. M.; Giammona, G. Branched High Molecular Weight Glycopolypeptide With Broad-Spectrum Antimicrobial Activity for the Treatment of Biofilm Related Infections. ACS Appl. Mater. Interfaces 2018, 10, 318–331.
- (48) Nkazi, B. D.; Neuse, E. W.; Aderibigbe, B. A. Polymeric Co-Conjugates of Curcumin. *J. Inorg. Organomet. Polym. Mater.* **2012**, 22, 886–891.
- (49) Dang, Q. D.; Park, J. H.; Bhang, S. H.; Kim, J.-H. Synthesis and characterization of novel multi-hydroxy polyaspartamide derivative and its crosslinked hydrogels. *React. Funct. Polym.* **2020**, *147*, 104455.
- (50) Fu, L.; Lv, J.; Zhou, L.; Li, Z.; Tang, M.; Li, J. Study on corrosion and scale inhibition mechanism of polyaspartic acid grafted  $\beta$ -cyclodextrin. *Mater. Lett.* **2020**, 264, 127276.
- (51) Lim, C.; Kim, D. w.; Kim, D. Bone targeting nano-aggregates prepared from self-assembled polyaspartamide graft copolymers for pH sensitive DOX delivery. *Biomater. Sci.* **2021**, *9*, 1660–1667.
- (52) Wang, M.; Zhang, H.; Wang, H.; Feng, H.; Deng, H.; Wu, Z.; Lu, H.; Li, Z. Development of [18F] AlF-NOTA-NT as PET agents of neurotensin receptor-1 positive pancreatic cancer. *Mol. Pharmaceutics* **2018**, *15*, 3093–3100.

## **□** Recommended by ACS

Near-Infrared Light-Activated Dual Targeting with Peptide-Conjugated Mesoporous Silica Nanoparticles for Multimodal Anticancer Therapy

Karunanidhi Gowsalya, Raju Vivek, et al.

NOVEMBER 01, 2022

ACS APPLIED NANO MATERIALS

DEAD E

Unfolding the Potency of Adenosine in Targeting Triple Negative Breast Cancer via Paclitaxel-Incorporated pH-Responsive Stealth Liposomes

Dasharath Chaudhari, Sanyog Jain, et al.

JULY 27, 2022

ACS BIOMATERIALS SCIENCE & ENGINEERING

READ 🗹

Subcellular-Targeted Near-Infrared-Responsive Nanomedicine with Synergistic Chemo-photothermal Therapy against Multidrug Resistant Cancer

Zhaomin Tang, Xia Luo, et al.

MARCH 21, 2022

MOLECULAR PHARMACEUTICS

READ 🗹

Biotin-Targeted Multifunctional Nanoparticles Encapsulating 10-Hydroxycamptothecin and Apoptin Plasmid for Synergistic Hepatocellular Carcinoma Treat...

Zhuanxia He, Xiujun Gao, et al.

DECEMBER 06, 2021

ACS APPLIED POLYMER MATERIALS

READ 🗹

Get More Suggestions >